Temporal variation and frequency dependence of ambient noise on Mars from polarization analysis

Yudai Suemoto[1], Takeshi Tsuji[1,2] *, Tatsunori Ikeda[1,2]

[1] Department of Earth Resources Engineering, Kyushu University, 744 Motooka, Nishi-ku, Fukuoka 819-0395, Japan

[2] International Institute for Carbon-Neutral Energy Research (WPI-I2CNER), Kyushu University, 744 Motooka, Nishi-ku, Fukuoka 819-0395, Japan

Corresponding author: Takeshi Tsuji (tsuji@mine.kyushu-u.ac.jp)

Key points:

- A polarization analysis of InSight seismic data enables estimates of temporal variation and frequency dependence of ambient noise on Mars.
- Higher-frequency (4–8 Hz) P-waves and Rayleigh waves show diurnal variation of back-azimuth that may be induced by wind and temperature.
- Changes in the trend of Rayleigh waves below 0.25 Hz may be related to a lithological boundary as well as variations in ambient noise.

Abstract

We applied a polarization analysis of InSight seismic data to estimate temporal variation and frequency dependence of the Martian ambient noise field. An autocorrelation analysis suggests that a lithological boundary beneath the seismometer influences ambient noise characteristics. High-frequency (4–8 Hz) P-waves show a diurnal variation in the dominant back-azimuth that appears to be related to wind and direction of sunlight in a distant area. High-frequency Rayleigh waves (4–8 Hz) also show diurnal variation and a dominant back-azimuth related to wind direction in a nearby area. Rayleigh waves of <2 Hz show diurnal variations. However, the dominant back-azimuths of P-waves of <4 Hz and Rayleigh waves of 2–4 Hz are constant. Therefore, the higher frequency signal could be derived mainly from wind. These results point to the presence of several ambient noise sources as well as site amplification effects related to geologic structure at the InSight landing site.

Plain Language Summary

Ambient seismic noise (microtremors) is continuously generated not only on Earth but also on Mars. We used data from the seismometer on the InSight lander to make estimates of microtremor characteristics and identified possible underground structures that influence the propagation of microtremors. High-frequency P-waves derived from microtremors show daily variations that appear to be induced by wind and changes of sunlight during the Martian day in distant areas, whereas high-frequency Rayleigh waves show daily variations that may be generated by wind in nearby areas. Microtremors in other frequency ranges have different characteristics. These results suggest that depending on their frequency, microtremors can be induced by wind and other sources, and may then be influenced by geological structures. Ambient noise data will be helpful for imaging and monitoring Mars' interior structure and natural resources, such as ice deposits, without the need for data from marsquakes and artificial seismic sources.

Keywords: InSight, ambient noise, polarization analysis, autocorrelation function, wind

1. Introduction

When NASA's Interior Exploration using Seismic Investigations, Geodesy and Heat Transport (InSight) lander touched down in Elysium Planitia on 26 November 2018, it went on to deploy the first complete geophysical observatory on Mars. One of its primary scientific investigations is the Seismic Experiment for Interior Structure (SEIS; InSight Mars SEIS Data Service, 2019). The lander also includes a set of environmental sensors, including temperature and wind sensors (Banfield et al., 2019; Spiga et al., 2018). The InSight seismometer has detected several hundred marsquakes, most of them much smaller than earthquakes typically felt on Earth, but some were nearly as large as magnitude 4 (Witze, 2019). The instrument is especially sensitive to seismic events at night, when the strong ambient noise generated during the day by wind is subdued (Witze, 2019).

Analysis of ambient seismic noise is a technique widely used on Earth to image and monitor the subsurface (e.g., Nimiya et al., 2017; Nishida et al., 2008), and several studies have made similar use of ambient noise on the Moon (e.g., Larose et al., 2005; Tanimoto et al., 2008). If ambient noise can be used to image and monitor the interior structures of Mars, this technique will be a powerful tool because it does not require any natural marsquakes or artificial seismic sources.

In this paper, we characterize the ambient noise on Mars relying mainly on data from the InSight seismometer. We applied a polarization analysis to the InSight seismic records (InSight Mars SEIS Data Service, 2019) to extract the dominant back-azimuth and directional intensity of ambient noise. Furthermore, by comparing the characteristics of Rayleigh waves with autocorrelation functions (i.e., reflectivity), we achieved some insight into the relationship between lithology and ambient noise characteristics. By demonstrating the feasibility of ambient noise methods on Mars, this study shows that future seismic network projects on Mars will contribute to not only modeling and monitoring of Mars' interior structure, but also exploration for Martian resources, especially ice deposits.

2. Data and Method

2.1. Data Preparation

The SEIS instrument includes a long-period, very broad band seismometer (SEIS-VBB) with a sampling rate of 20 Hz (Lognonné et al., 2019; InSight Mars SEIS Data Service, 2019). This seismometer was placed in Elysium Planitia in particular to satisfy the constraints on landing safety and the instrument deployment requirements (Golombek et al., 2017). In this study, we used continuous seismic records from SEIS-

VBB between February and June 2019. The SEIS-VBB is a triaxial seismometer in which the three mutually perpendicular pendulums are mounted obliquely. Therefore our first step was to numerically rotate the axes of the seismometer and construct seismic records with vertical and horizontal components (see supplementary information).

We then converted the seismic data from Earth time (UTC; Coordinated Universal Time) to the Mars time domain (LMST: Local Mean Solar Time) by using the procedures of Allison (1997) and Allison and McEwen (2000). The power spectra of the horizontal and vertical components from Sols 194 to 197 (**Fig. 1**) are an example of the typical daily cycle, in which signal amplitudes are greater during the day than during the night. These results demonstrate that the amplitude of ambient noise is strongly correlated with the wind strength.

2.2. Polarization Analysis

In this analysis, we divided continuous seismic data into 1-min segments. We excluded time segments whose root-mean-squared (RMS) amplitudes exceeded 10 times the median RMS amplitude, treating daytime hours (from 6:00 to 18:00 LMST) and nighttime hours (from 18:00 to 6:00 LMST) separately because the surface wind velocity was anticipated to be very high (15–20 m/s) during the daytime at the InSight landing site (Spiga et al., 2018). We conducted a polarization analysis of the ambient noise seismic field recorded by the InSight station using the method developed by Takagi et al. (2018). This analysis uses a simple relationship between the vertical-horizontal cross spectra and the azimuthal energy distributions of incident waves in ambient noise. The real part of the cross spectra is related to P-waves and the imaginary part is related to Rayleigh waves. We computed vertical-horizontal cross spectra using the equations

$$\Phi_{ZN} = \frac{u_Z^* u_N}{u_Z^* u_Z}, \tag{1}$$

$$\Phi_{ZE} = \frac{u_Z^* u_E}{u_Z^* u_Z}, \tag{2}$$

where Φ is the vertical-horizontal cross spectrum, u is the seismic record in the frequency domain of each component, and the asterisk indicates the conjugate. The cross spectra are normalized by the power spectra of the vertical component so as to equally weight each data segment. In this study, the cross spectra were calculated at each frequency and the results were averaged within each of six single-octave frequency bands: 0.125–0.25, 0.25–0.5, 0.5–1, 1–2, 2–4 and 4–8 Hz.

Following Takagi et al. (2018), the dominant direction and directional intensity of a Rayleigh wave are given by

$$\varphi_{R1} = arctan\left(\frac{Im\langle\Phi_{ZN}\rangle}{Im\langle\Phi_{ZE}\rangle}\right) + \pi, \tag{3}$$

$$A_{R1} = \sqrt{(Im\langle\Phi_{ZN}\rangle)^2 + (Im\langle\Phi_{ZE}\rangle)^2}, \tag{4}$$

and for a P-wave by

$$\varphi_{P1} = arctan\left(\frac{Re\langle\Phi_{ZN}\rangle}{Re\langle\Phi_{ZE}\rangle}\right) + \pi, \tag{5}$$

$$A_{P1} = \sqrt{(Re\langle\Phi_{ZN}\rangle)^2 + (Re\langle\Phi_{ZE}\rangle)^2}, \tag{6}$$

where $\langle\rangle$ denotes the ensemble average, φ_{R1} and φ_{P1} represent the phase angles of first-order terms of the azimuth spectra added to π, which provide the dominant back-azimuths of Rayleigh waves and P-waves, respectively. A_{R1} and A_{P1} indicate the amplitudes of the first-order terms representing the intensity of the directionality of the Rayleigh wave and P-wave, respectively.

2.3. Autocorrelation Analysis

To estimate the geological structure beneath the InSight landing site, we applied autocorrelation analysis to the vertical and horizontal motions of the seismometer record. Autocorrelation of ambient noise records yields the zero-offset shot gather (e.g., Minato et al., 2012; Wapenaar & Fokkema, 2006). The method assumes that the noise source is randomly distributed, and mutually uncorrelated for different source positions (e.g., Roux et al., 2005; Wapenaar and Fokkema, 2006; Weaver & Lobkis, 2004). In this analysis, we divided continuous seismic data during the same period of polarization analysis (from February to June 2019) into 1-h segments. We applied a bandpass filter of 5–7 Hz to each component record. We applied one-bit normalization (e.g., Bensen et al., 2007) to ensure the exclusion of energetic signals. We calculated autocorrelation functions of the vertical component and the horizontal components in each Sol to extract P- and S-wave reflections, respectively.

3. Results

Fig. 2a and 2b show the temporal variations of dominant back-azimuths and directional intensity of P-waves and Rayleigh waves from Sols 75 to 210 in the six frequency bands. The cross spectra are averaged for each LMST hour. The dominant back-azimuths were different for each frequency band. The directional intensity of Rayleigh waves was less than that of P-waves in all frequency bands.

To illustrate the daily temporal variation, we present results from Sols 194 to 197 (**Fig. 3a and 3b**). In most frequency ranges, the dominant back-azimuths and directional intensity of P-waves (**Fig. 3a**) did not vary much. The dominant back-azimuths of 0.125–1 Hz P-waves were to the west; however, at 4–8 Hz, the back-azimuths shifted from east to west during the course of the day, roughly consistent with the wind direction. At night, the back-azimuth of P-waves was unstable as wind strengths were weak. More precisely, the back-azimuth of high-frequency P-waves differed slightly from the wind direction at night, pointing east several hours before sunrise and pointing west after sunset.

For Rayleigh waves, the back-azimuths and directional intensity both varied over the course of the day, but the variation differed for the different frequency bands (**Fig. 3b**). For waves lower than 2 Hz, the back-azimuths were dominantly northeast or east at night and northwest or west during the day. At 0.125–0.25 Hz, the back-azimuths and directional intensity of Rayleigh waves did not show a clear diurnal pattern. At 2–4 Hz, the dominant back-azimuth was almost constant, pointing between south and west. At 4–8 Hz, the back-azimuth pointed south during the day and west at night, similar to the wind direction. In addition to intensity of Rayleigh waves included in ambient noise, a layered medium beneath the seismometer is also responsible for the frequency dependence of the estimated intensity of Rayleigh waves (**Fig. 3b**), as we discuss in the following section.

Fig. 4 shows the temporal variation of the autocorrelation function during the observation period. The autocorrelation function of the vertical component (**Fig. 4a**) indicates the presence of reflectors at 0.6 s and 1.1 s. Because the reflectors at 0.6 and 1.1 s persisted throughout the observation period, they appear to be reliable and may represent a lithological boundary that imposes a contrast in acoustic impedance. The autocorrelation functions of the two horizontal components (**Fig. 4b and 4c**) display multiple reflectors from 0.5 to 2.4 s. They show evidence of anisotropy, in that the reflector at ~1.1 s is more prominent in the EW component (**Fig. 4c**) than in the NS component (**Fig. 4b**).

4. Discussion

The temporal variation of the dominant back-azimuth of 4–8 Hz P-waves could be related to the direction of sunlight (or related thermal effects) in addition to the wind direction. During the several hours before sunrise, the area east of the landsite is in daylight and the wind speed is high, thus the dominant P-wave back-azimuth could point east before sunrise (**Fig. 3a**). This interpretation would also explain the westward P-wave back-azimuth after sunset. These results demonstrate that high-frequency P-waves observed near the InSight site may be derived from wind and insolation effects in distant areas. Indeed, P-waves on Earth are strongly influenced by distant events (Takagi et al., 2018). Seismic sources induced by temperature variation are capable of generating high-frequency ambient noise. In contrast, the dominant back-azimuths of P-waves at lower frequencies (<4 Hz) were constant and pointed between south and west.

The variation of the directionality of 4–8 Hz Rayleigh waves was strongly related to the wind direction, except during periods of weak wind (**Fig. 3b**). Therefore, high-frequency Rayleigh waves may be derived from winds close to the seismometer. Rayleigh waves of higher frequency (4–8 Hz) would be sensitive to the depth range of 6.25–12.5 m, if we assume a Rayleigh wave velocity of 150 m/s (Knapmeyer-Endrun et al., 2017). Therefore, Rayleigh waves that are sensitive to subsurface formations shallower than ~12.5 m should be much influenced by short-term variations of the wind. Although the dominant back-azimuths of Rayleigh wave at 2–4 Hz ranged from south to west, diurnal variations also appeared in Rayleigh waves <2 Hz, in which the back-azimuths pointed northwest during the day and northeast at night.

These frequency-dependent variations of ambient noise characteristics could be mainly related to ambient noise sources. Ambient noise on Earth is caused by wind (Lepore et al., 2016) as well as ocean tides, volcanic activity, and anthropogenic sources (e.g., Takagi et al., 2018; Nimiya et al., 2017). Before the InSight project, a main source of ambient noise on Mars was expected to be the direct interaction between the atmosphere and the solid surface of the planet (Knapmeyer-Endrun et al., 2017). On the Moon, high-frequency Rayleigh waves are induced by ambient noise resulting from thermal events (Larose et al., 2005; Tanimoto et al., 2008). On Mars, there are numerous small craters near the InSight landing site (Warner et al., 2016) that could be locations of thermally triggered soil slumping (Knapmeyer-Endrun et al., 2017) that could generate high-frequency surface waves. Thus wind, thermal effects, surface pressure, or other sources may induce the ambient noise around the InSight landing area.

The frequency dependence of the intensity of Rayleigh waves (**Fig. 3b**) may also be related to the lithology of the site, because a layered medium acts as a frequency-dependent filter (e.g., Scherbaum et al., 2003). Several reflectors beneath the InSight landing site are evident from the autocorrelation results (**Fig. 4**). The P-wave reflectors at 0.6 and 1.1 s in the vertical component (**Fig. 4a**) are stable, suggesting the existence of a significant lithological boundary. Furthermore, an S-wave reflector appeared at 1.1 s in the horizontal component results (**Fig. 4b and 4c**). If the 1.1 s S-wave reflector is the same as the 0.6 s P-wave reflector, we can estimate the ratio of ~1.83 between the P-wave and S-wave velocities. Because we cannot estimate the seismic velocity of the subsurface formation, we cannot accurately estimate the depth of the reflectors from the autocorrelation functions. However, we can estimate the frequency of Rayleigh waves that are sensitive to the depth of a reflector from the autocorrelation function. Under the assumption that the autocorrelation function of the horizontal component represents S-wave reflectivity, the depth of a reflector at two-way travel time t can be estimated as $Z = t\,V_S/2$, where V_S is S-wave velocity. The sensitive depth of Rayleigh waves is $Z = 1/3\ \lambda$ (or $Z = V_S/3f$) (e.g., Foti et al., 2014; Hayashi, 2008), where λ is wavelength and f is frequency. Therefore, the sensitive frequency of a Rayleigh wave for a reflector at two-way travel time t can be estimated as $f = 2/(3t)$. From this relationship, the frequency of a Rayleigh wave that is sensitive to a 1.1 s reflector shown in **Fig. 4b and 4c** can be estimated as ~0.3 Hz. Indeed, below 0.25 Hz, the azimuth and intensity of Rayleigh waves are scattered in comparison to those at higher frequencies (**Fig. 3b**). Therefore, it might be possible that the influence of a lithological boundary can be detected in the temporal variation (or stability) of the back-azimuth and intensity of Rayleigh waves.

5. Conclusions

We have conducted a polarization analysis of InSight seismic data to estimate temporal variations of the ambient noise field on Mars. Our findings are these:

- High-frequency (4–8 Hz) P-waves show a diurnal variation, and the dominant back-azimuth is related to the wind and the direction of sunlight in distant regions.
- High-frequency (4–8 Hz) Rayleigh waves show a diurnal variation, and the dominant back-azimuth points toward the wind direction in nearby regions.
- Rayleigh waves of frequencies lower than 2 Hz show periodic variations in back-azimuth and directional intensity, whereas P-waves of frequencies lower than 4 Hz have constant back-azimuths.

These results suggest that the dominant sources of ambient noise on Mars differ with frequency and wave type, and there may be several different ambient noise sources despite the absence of oceans on Mars. Furthermore, the lithological boundary identified from the autocorrelation analysis may impose a site effect upon the ambient noise characteristics. The high repeatability of P-waves and Rayleigh waves derived from ambient noise suggests the feasibility of utilizing ambient noise for subsurface imaging and monitoring on Mars.

Acknowledgement

We acknowledge NASA, CNES, their partner agencies and Institutions (UKSA, SSO, DLR, JPL, IPGP-CNRS, ETHZ, IC, MPS-MPG) and the flight operations team at JPL, SISMOC, MSDS, IRIS-DMC and PDS for providing SEED SEIS data. The seismometer data was downloaded from the following URLs; http://service.iris.edu/fdsnws/dataselect/docs/1/builder/, and https://www.seis-insight.eu/en/science/seis-data/seis-data-availability. The wind and temperature data was downloaded from the following URL; https://atmos.nmsu.edu/data_and_services/atmospheres_data/INSIGHT/insight.html#Selecting_Data.

References

Allison, M. (1997). Accurate analytic representations of solar time and seasons on Mars with applications to the Pathfinder/Surveyor missions. *Geophysical Research Letters*. https://doi.org/10.1029/97GL01950

Allison, M., & McEwen, M. (2000). A post-Pathfinder evaluation of areocentric solar coordinates with improved timing recipes for Mars seasonal/diurnal climate studies. *Planetary and Space Science*, *48*(2–3), 215–235. https://doi.org/10.1016/s0032-0633(99)00092-6

Banfield, D., Rodriguez-Manfredi, J. A., Russell, C. T., Rowe, K. M., Leneman, D., Lai, H. R., et al. (2019). InSight Auxiliary Payload Sensor Suite (APSS). Space Science Reviews (Vol. 215). *Springer Nature B.V.* https://doi.org/10.1007/s11214-018-0570-x

Bensen, G. D., Ritzwoller, M. H., Barmin, M. P., Levshin, A. L., Lin, F., Moschetti, M. P., et al. (2007). Processing seismic ambient noise data to obtain reliable broad-band surface wave dispersion measurements. *Geophysical Journal International*, *169*(3), 1239–1260. https://doi.org/10.1111/j.1365-246X.2007.03374.x

Foti, S., Lai, G. C., Rix, G. J., & Strobbia, C. (2014). Surface wave methods for near-surface site characterization. London: CRC Press. https://doi.org/10.1201/b17268

Golombek, M., Kipp, D., Warner, N., Daubar, I. J., Fergason, R., Kirk, R. L., et al. (2017). Selection of the InSight Landing Site. *Space Science Reviews*, *211*(1–4), 5–95. https://doi.org/10.1007/s11214-016-0321-9

Hayashi, K. (2008). Development of surface-wave methods and its application to site investigations: Ph.D. dissertation, Kyoto University.

Knapmeyer-Endrun, B., Golombek, M. P., & Ohrnberger, M. (2017). Rayleigh Wave Ellipticity Modeling and Inversion for Shallow Structure at the Proposed InSight Landing Site in Elysium Planitia, Mars. *Space Science Reviews*, *211*(1–4), 339–382. https://doi.org/10.1007/s11214-016-0300-1

Larose, E., Khan, A., Nakamura, Y., & Campillo, M. (2005). Lunar subsurface investigated from correlation of seismic noise. *Geophysical Research Letters*, *32*(16), 1–4. https://doi.org/10.1029/2005GL023518

Lepore, S., Markowicz, K., & Grad, M. (2016). Impact of wind on ambient noise recorded by seismic array in northern Poland. *Geophysical Journal International*, *205*(3), 1406–1413. https://doi.org/10.1093/gji/ggw093

Lognonné, P., Banerdt, W. B., Giardini, D., Pike, W. T., Christensen, U., Laudet, P., et al. (2019). SEIS: Insight's Seismic Experiment for Internal Structure of Mars. *Space Science Reviews* (Vol. 215). The Author(s). https://doi.org/10.1007/s11214-

018-0574-6

Minato, S., Tsuji, T., Ohmi, S., & Matsuoka, T. (2012). Monitoring seismic velocity change caused by the 2011 Tohoku-oki earthquake using ambient noise records. *Geophysical Research Letters*, *39*(9), 1–6. https://doi.org/10.1029/2012GL051405

Nimiya, H., Ikeda, T., & Tsuji, T. (2017). Spatial and temporal seismic velocity changes on Kyushu Island during the 2016 Kumamoto earthquake. *Science Advances*, *3*(11). https://doi.org/10.1126/sciadv.1700813

Nishida, K., Kawakatsu, H., & Obara, K. (2008). Three-dimensional crustal S wave velocity structure in Japan using microseismic data recorded by Hi-net tiltmeters. *Journal of Geophysical Research: Solid Earth*, *113*(10), 1–22. https://doi.org/10.1029/2007JB005395

Rodriguez-Manfredi, J.A. et al., InSight APSS TWINS Data Product Bundle, urn:nasa:pds:insight_twins, 2019.

Roux, P., Sabra, K. G., Kuperman, W. A., & Roux, A. (2005). Ambient noise cross correlation in free space: Theoretical approach. *The Journal of the Acoustical Society of America*, *117*(1), 79–84. https://doi.org/10.1121/1.1830673

Spiga, A., Banfield, D., Teanby, N. A., Forget, F., Lucas, A., Kenda, B., et al. (2018). Atmospheric Science with InSight. *Space Science Reviews* (Vol. 214). Springer Nature B.V. https://doi.org/10.1007/s11214-018-0543-0

Scherbaum, F., Hinzen, K. G., & Ohrnberger, M. (2003). Determination of shallow shear wave velocity profiles in the cologne, Germany area using ambient vibrations. Geophysical Journal International, 152(3), 597–612. https://doi.org/10.1046/j.1365-246X.2003.01856.x

Takagi, R., Nishida, K., Maeda, T., & Obara, K. (2018). Ambient seismic noise wavefield in Japan characterized by polarization analysis of Hi-net records. *Geophysical Journal International*, *215*(3), 1682–1699. https://doi.org/10.1093/gji/ggy334

Tanimoto, T., Eitzel, M. V., & Yano, T. (2008). The noise cross-correlation approach for Apollo 17 LSPE data: Diurnal change in seismic parameters in shallow lunar crust. *Journal of Geophysical Research E: Planets*, *113*(8), 1–12. https://doi.org/10.1029/2007JE003016

Wapenaar, K., & Fokkema, J. (2006). Green's function representations for seismic interferometry. *Geophysics*, *71*(4). https://doi.org/10.1190/1.2213955

Warner, N. H., Golombek, M. P., Sweeney, J., Pivarunas, A., & Survey, U. S. G. (2016). 47th Lunar and Planetary Science Conference (2016) REGOLITH THICKNESS ESTIMATES FROM THE SIZE FREQUENCY DISTRIBUTION

OF ROCKY 47th Lunar and Planetary Science Conference (2016), 5–6.

Weaver, R. L., & Lobkis, O. I. (2004). Diffuse fields in open systems and the emergence of the Green's function (L). *The Journal of the Acoustical Society of America*, *116*(5), 2731–2734. https://doi.org/10.1121/1.1810232

Witze, A. (2019). "Marsquakes" reveal red planet's hidden geology. *Nature*, *576*(7787), 348. https://doi.org/10.1038/d41586-019-03796-7

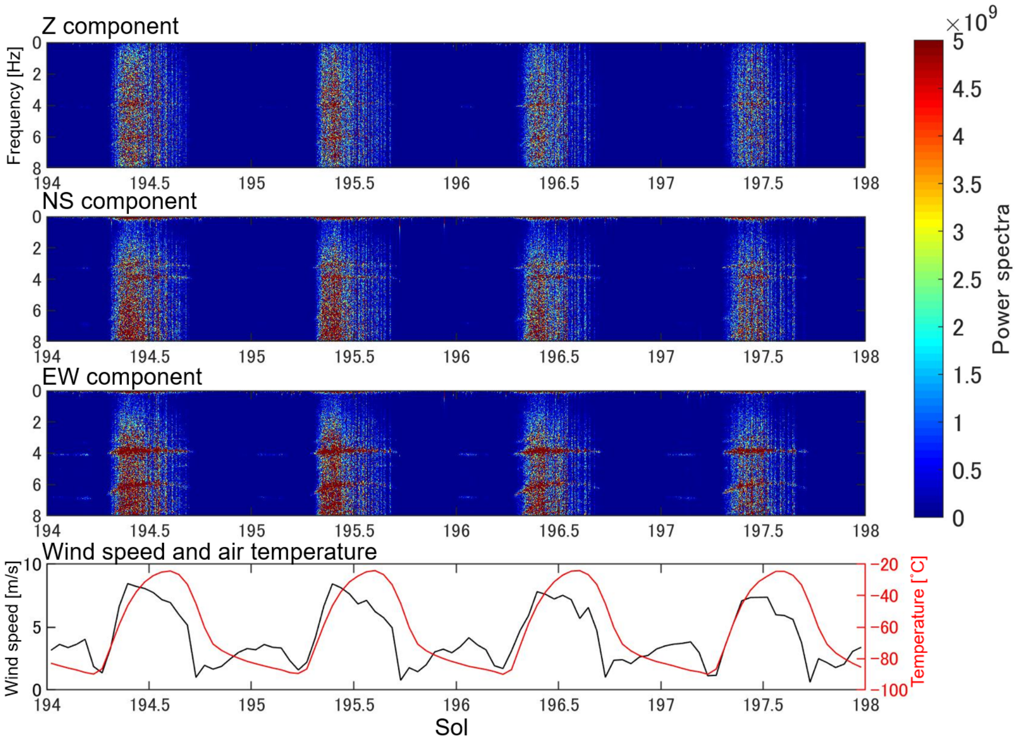

Fig. 1. Temporal variation of power spectra in the vertical and two horizontal components from Sols 194 to 197. The bottom figure shows the temporal variation of wind speed and air temperature.

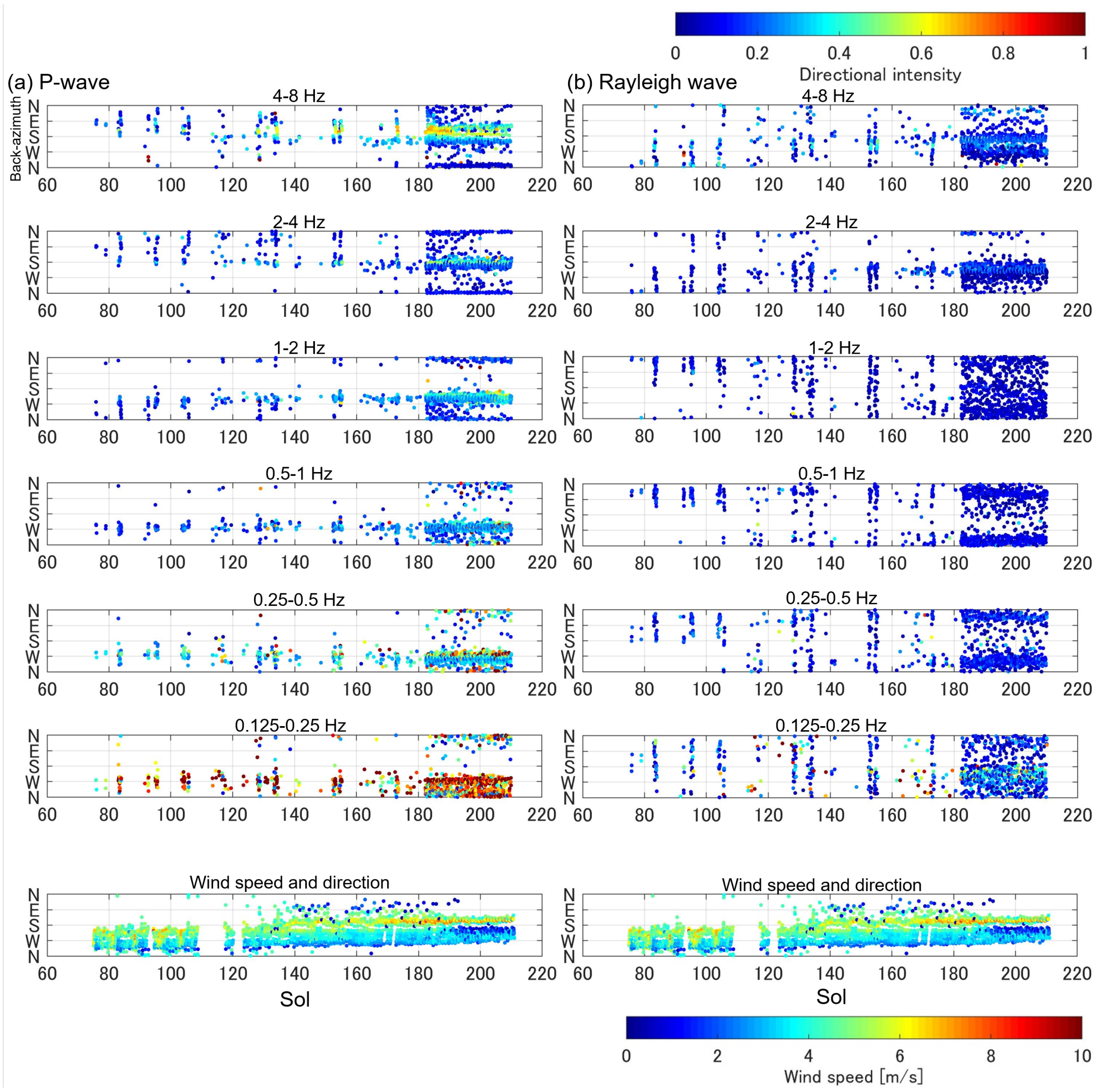

Fig. 2. Temporal variation of dominant back-azimuths and directional intensity of (a) P-waves and (b) Rayleigh waves in six single-octave frequency bands between Sols 75 and 210. The bottom figure shows the wind speed and direction during the same period.

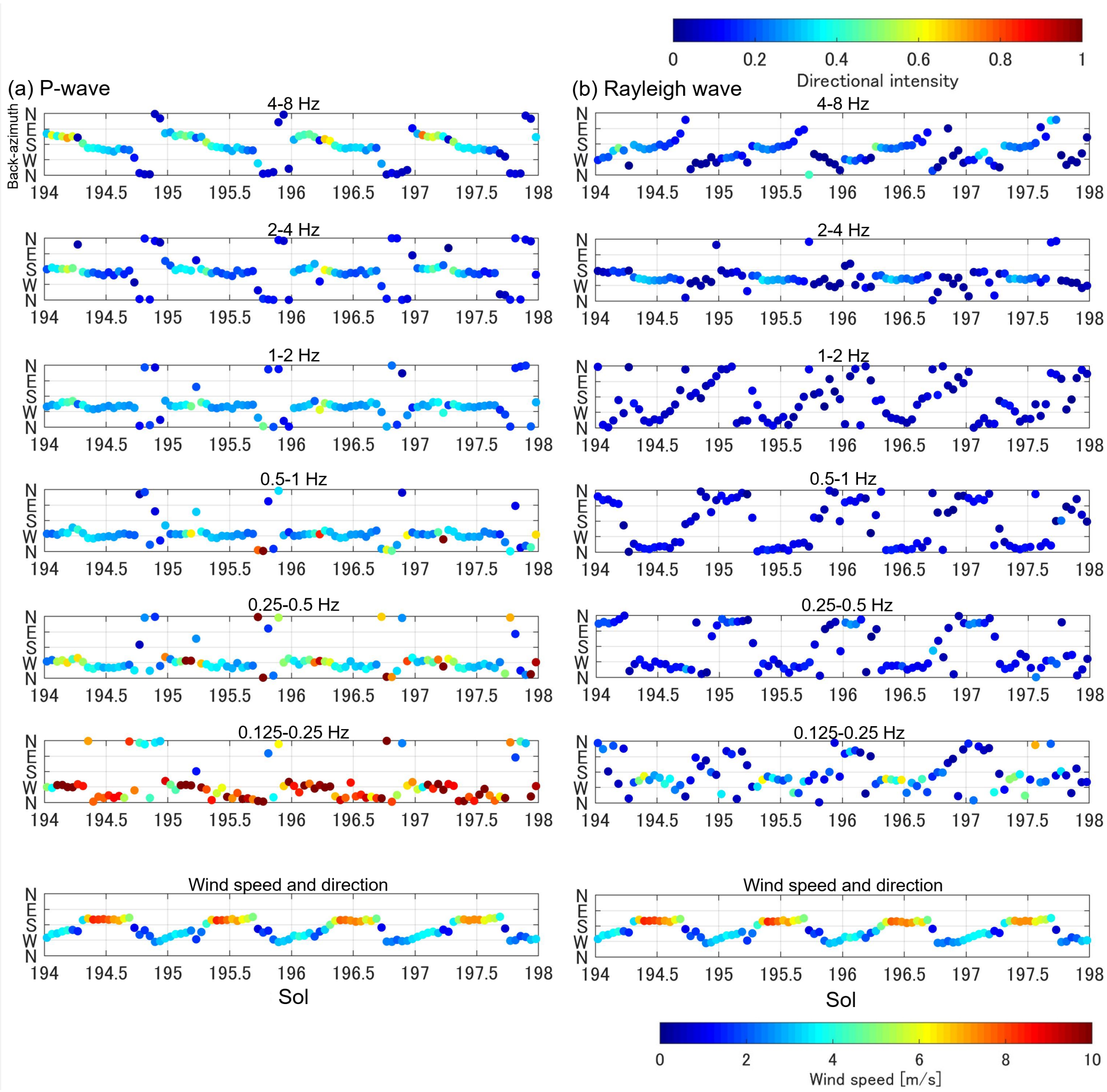

Fig. 3. Temporal variations from Sols 194 to 197 in the dominant back-azimuths and directional intensity of (a) P-wave and (b) Rayleigh wave. The bottom figure shows the wind speed and direction during the same period.

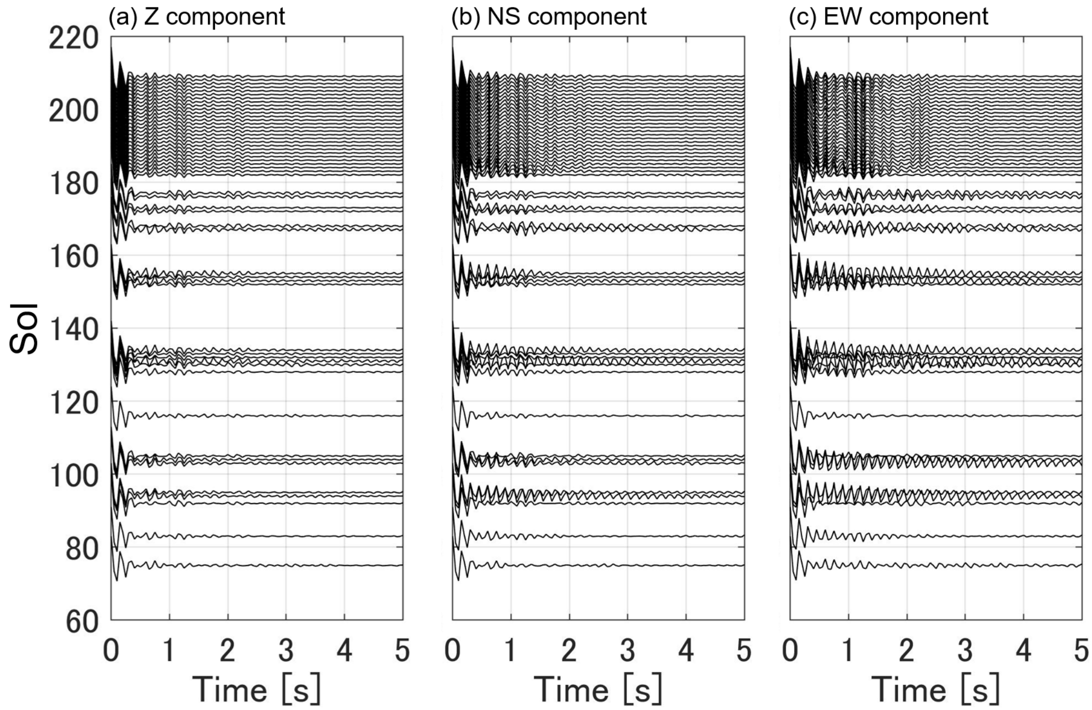

Fig. 4. Temporal variation of autocorrelation functions of components from Sols 75 to 210: (a) Vertical component; (b) NS component; (c) EW component. The vertical component could be similar to P-wave reflectivity whereas the NS and EW components could be S-wave reflectivity.